ACS Catalysis

pubs.acs.org/acscatalysis
Research Article

Boosting the Electroreduction of Nitrate to Ammonia in a PEM Electrolyzer with Polymer-Modified Ru Nanoparticles

Min Li,[‖] Jinghan Zhao,[‖] Vineesh Thazhe Veettil, Shilong Fu, Ahmed Mohsen Ismail, Ruud Kortlever, and Atsushi Urakawa*

Cite This: ACS Catal. 2026, 16, 3430−3441
Read Online

ACCESS | Metrics & More | Article Recommendations | Supporting Information

ABSTRACT: Ammonia (NH_3) is vital for synthesizing fertilizers and has gained great attention as a carbon-free hydrogen carrier and a hydrogen-rich fuel. Electrochemical ammonia synthesis from nitrate in a water-fed polymer electrolyte membrane electrolyzer is an innovative approach to wastewater treatment. However, the major hurdles to practical implementation are competing hydrogen evolution reactions (HERs) and constrained catalytic efficiency. Herein, we demonstrate the use of polyvinylpyrrolidone (PVP)-modified ruthenium (Ru) nanoparticles as a strategy to drive the desired reaction of nitrate to ammonia. The particle size of Ru was controlled by PVP, enhancing the metal-utilization efficiency and the electrochemical active surface area. PVP modification was found to alter the electron density on Ru, suppressing the HER by increasing the energy barrier of hydrogen coupling to form H_2, while promoting absorbed hydrogen (H*) formation, facilitating the hydrogenation of intermediates to ammonia. Benefiting from the combined effects, PVP-10 wt % Ru/C achieved an ammonia production rate of 3800 $\mu g \cdot mg_{Ru}^{-1} \cdot h^{-1}$, compared to 590 $\mu g \cdot mg_{Ru}^{-1} \cdot h^{-1}$ for 40 wt % Ru/C at 2 V.

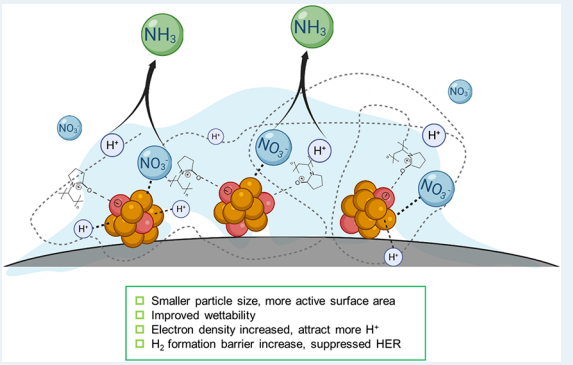

KEYWORDS: *electrocatalyst, ammonia synthesis, nitrate reduction, PEM cell, capping ligand, hydrogen binding energy*

INTRODUCTION

Nitrogen is the fifth most abundant element on Earth and is a crucial nutrient element for all living organisms.[1] The increased use of fertilizers has resulted in global environmental pollution and an energy crisis. Particularly, plants absorb only about 40% of the applied fertilizer, with the rest remaining in the soil.[2] This leftover ammonium (NH_4^+) is converted into nitrate (NO_3^-) by soil bacteria.[3,4] The soluble NO_3^- can leach into aquatic systems, causing eutrophication, acidification, and ecosystem disturbances.[5,6] Numerous technologies have been developed for the removal of nitrate from groundwater, including chemical and biological denitrification, reverse osmosis, ion-exchange processes, and electrocatalytic denitrification.[7] Among these, the electrochemical nitrate reduction reaction (NO_3RR) has emerged as a promising approach for both wastewater treatment and ammonia synthesis.[8−10] This process is a promising alternative to the conventional energy-intensive Haber−Bosch process[11,12] which involved high-energy consumption (1−2% of globally available energy annually[13]) and large amounts of CO_2 emission (1−1.5% of global emissions).[14]

However, a principal challenge in this eight-electron-transfer process is achieving high selectivity toward ammonia against the competing hydrogen evolution reaction (HER).[15,16] This competition arises mechanistically from the involvement of the surface-absorbed active hydrogen (*H), which is generated on the catalyst via the initial Volmer step ($H_2O + * + e^- \rightarrow *H + OH^-$).[17] This *H species is fundamentally important as it serves as the hydrogenating agent for the sequential reduction of nitrate to ammonia. However, the accumulation of *H also promotes the HER through two competing pathways: the Tafel step ($*H + *H \rightarrow H_2 + 2*$),[18] involving the recombination of two adsorbed *H intermediates, or the Heyrovsky step ($*H + H^+ + e^- \rightarrow H_2 + *$), where an *H intermediate reacts with a proton−electron pair.[19] Consequently, the catalytic surface kinetics dictate a delicate balance: insufficient *H coverage limits the NO_3RR rate, whereas excessive coverage kinetically favors H_2 evolution, thereby diminishing the Faradaic efficiency toward ammonia synthesis.

Therefore, great efforts have been devoted to catalyst development for this process aiming to suppress the HER while facilitating efficient NO_3RR. One effective approach is to modulate the electronic structure of the catalyst to weaken

Received: October 27, 2025
Revised: January 4, 2026
Accepted: January 5, 2026
Published: February 11, 2026

hydrogen (*H) binding, which could selectively promote the nitrate hydrogenation while suppressing the competing HER.[20−26] Another promising approach is to use bifunctional catalysts that have separate active sites—one designed for adsorbing and activating nitrate and another for hydrogenation.[27,28] Thus, deeper knowledge of the competitive interplay between the NO_3RR and HER intermediates, along with the specific behavior of *H, remains essential for future catalyst design breakthroughs. To achieve high performance in the NO_3RR, it is crucial not only to focus on the suppression of the HER but also to increase the number of active sites for the reaction, especially when using costly noble metals like ruthenium.[29,30] One effective strategy to solve this problem is to decrease the metal loading while downsizing the particle to increase the active surface area, which is a straightforward way to improve the catalytic activity with economic advantages.[31−34]

Meanwhile, currently, most studies aiming at developing efficient electrocatalysts are conducted on H-cells or batch cells that cannot be operated continuously and hinder the commercialization and large-scale operation.[35] Thus, performing the NO_3RR in a continuous manner using a membrane electrode assembly (MEA) electrolyzer is a promising approach which can significantly reduce the internal Ohmic resistances and improve the energy efficiency.[36,37] Recently, the electrochemical nitrate reduction to ammonia in an alkaline flow cell has been reported, but the electrolytes used are typically concentrated KOH solutions, which can cause serious corrosion problems and difficulties in device management.[38,39] Therefore, conducting electrochemical nitrate reduction in a polymer electrolyte membrane (PEM) flow cell with NO_3^--pure water coelectrolysis toward ammonia synthesis is a more practical approach for future large-scale application.

In this study, we report an unforeseen but profound HER suppression effects from the capping ligand polyvinylpyrrolidone (PVP, structure shown in Figure S1[40])-modified Ru nanoparticles (NPs). Specifically, we discovered that residual PVP, which is difficult to remove completely after synthesis, rather than inhibiting the reaction, critically enhances ammonia selectivity by suppressing the competing HER. Through detailed physical and electrochemical characterization, it can be concluded that PVP controls the particle size of Ru on the carbon support, which greatly enhances the metal-utilization efficiency and electrochemical active surface area (ECSA). Remarkably, PVP-modified 10 wt % Ru/C catalyst achieved an ECSA 4 times higher than that of a conventional 40 wt % Ru/C catalyst, despite the lower metal content. Additionally, PVP modulates the electron density on the Ru surface. This change increases the energy barrier for the coupling of adsorbed hydrogen (*H) to form H_2, thereby suppressing the HER while simultaneously promoting the formation of *H for the hydrogenation of reaction intermediates into ammonia. These insights reveal a simple and effective strategy for designing highly active and selective electrocatalysts for electrochemical nitrate reduction to ammonia.

EXPERIMENTAL METHODS

Synthesis of Different Ru Loadings on a Carbon Support

Ru NPs with different loadings (5, 10, 20, and 40 wt %) on a Vulcan XC72 carbon black support, named 5Ru/C, 10Ru/C, 20Ru/C, and 40Ru/C, respectively, were prepared by an impregnation reduction method with $NaBH_4$,[41] as shown in Figure S2. In a typical process with 40 wt % Ru/C as an example, 164.18 mg of $RuCl_3{\cdot}xH_2O$ (99.9%, Sigma-Aldrich) was dissolved in 50 mL of water in a round-bottom flask under stirring (1000 rpm). After 15 min, 120 mg Vulcan XC72 carbon black (Cabot Corporation) was added and stirred for 15 min at room temperature and then sonicated for another 30 min in an ultrasonic bath with additional ice to minimize heating. Subsequently, a freshly made $NaBH_4$ (Sigma-Aldrich) solution (179.67 mg, $NaBH_4$:Ru = 6:1, in moles, 6-fold excess with respect to the stoichiometric amount of Ru precursors) was slowly added dropwise into the suspension, followed by stirring for 1 h (1000 rpm) at room temperature. The catalyst was then collected and washed several times by centrifugation (6000 rpm and 15 min each cycle) with Milli-Q water to remove Na^+ and Cl^- ions. Finally, the catalyst was collected and dried in an oven at 80 °C overnight. 5, 10, and 20 wt % Ru/C catalysts were synthesized using the same method with different amounts of metal precursors and carbon black.

Synthesis of Different Ru Loadings on a Carbon Support with PVP

PVP-modified Ru NPs with different loadings (10, 20, and 40 wt %) supported on Vulcan XC72 carbon black, named PVP-10Ru/C, PVP-20Ru/C, and PVP-40Ru/C, respectively, were prepared by the same impregnation reduction method as described before. As shown in Figure S3, polyvinylpyrrolidone (PVP, MW = 40,000, Sigma-Aldrich) aqueous solution (PVP:Ru = 1.2:1, in w/w)[42] was added after the dissolution of $RuCl_3{\cdot}xH_2O$, and the remaining steps were kept the same as the previous Ru/C synthesis.

PVP Removal Experiment in PVP-10Ru/C

To exclude the possible effect of PVP itself on the electrocatalytic activity for the Ru/C catalyst, PVP removal was conducted for PVP-10Ru/C by heat treatment,[43,44] named PVP-10Ru/C-removed. Thermogravimetric analysis (TGA) of PVP (K30, MW = 40,000) was carried out in a Mettler Toledo SF/1100 thermogravimetric analyzer in a N_2 (100 mL·min^{-1}) inert atmosphere with a 2 °C·min^{-1} heating rate up to 800 °C. As shown in Figure S4, the results revealed that PVP decomposition starts at around 300 °C and finishes at around 660 °C. It is well known that the nanoparticles will coalesce when the stabilizing agent starts decomposing and will eventually form large agglomerations.[45,46] Thus, in order to remove PVP but avoid radical change to the morphology of the prepared PVP-10Ru/C, the catalyst was heat-treated at 300 °C with 2 °C·min^{-1} heating rate in N_2 (100 mL·min^{-1}) and kept for 8 h.

Material Characterization

Powder X-ray diffraction (XRD) was performed with a Bruker D8 Advance X-ray diffractometer using a Cu Kα radiation source in a range of 5 to 90° with a step of 0.05°. Transmission electron microscopy (TEM) images were taken with a JEOL JEM-1400 PLUS system to measure the surface morphology and particle size distributions. To study the surface chemical compositions and chemical states, X-ray photoelectron spectroscopy (XPS) was performed on a Thermo Scientific ESCLAB 250. The source used Al Kα radiation, and the mean X-ray photon energy was 1486.69 eV.

Membrane Electrode Assembly Preparation

The Nafion 115 membrane (Ion Power) was pretreated according to the activation procedure, by soaking for 1 h in 3 wt % hydrogen peroxide (H_2O_2, Sigma-Aldrich) solution at 80 °C, followed by 1 h in 1 M H_2SO_4 (Sigma-Aldrich) solution at 80 °C, and 1 h in boiling Milli-Q water. After the activation step, the membranes were stored in Milli-Q water to prevent swelling. 10 mg of the prepared cathode catalyst and 30 wt % Nafion ionomers (Nafion perfluorinated resin solution, Sigma-Aldrich) were ultrasonically dispersed in 2 mL of isopropanol for 30 min to generate a homogeneous ink. Then, the catalyst ink was spray-coated (Figure S5) onto a Nafion membrane with an active area of 2 × 2 cm^2 at 60 °C to obtain 2.5 mg·cm^{-2} catalyst loading. The anode ink was prepared by the same method consisting of 1.2 mg of commercial IrO_2 (0.3 mg·cm^{-2} catalyst loading), 20 wt % Nafion ionomer, and 2 mL of isopropanol. After spray coating, the catalyst-coated membranes (CCMs) were hot-

https://doi.org/10.1021/acscatal.5c07637
ACS Catal. 2026, 16, 3430−3441

pressed at 120 °C and 1 MPa for 3 min using an automatic press (Speca Press). The MEA was prepared by pressing two porous sintered titanium gas diffusion layers (2 × 2 cm^2) (GDL, Bekaert) on both sides of the membrane. The PEM electrolyzer was assembled by sandwiching the MEA, two titanium bipolar plates with flow channels, and two aluminum-cartridge-heated end plates with 5 N·m screw torque (Figure S6).

Electrochemical Nitrate Reduction Experiments

The electrochemical nitrate reduction experiments were conducted in a PEM electrolyzer (Figure S7) using an AUTOLAB PGSTAT302N potentiostat. The electrocatalytic performance of different loads of Ru/C catalysts for NO_3RR to ammonia was compared under ambient pressure at 80 °C where the electrolyzer was heated by heating cartridges. At the anode chamber, Milli-Q water was supplied, and at the cathode chamber, 1000 ppm of KNO_3 aqueous solution was supplied. For both chambers, the flow rate was set at 0.5 mL·min^{-1} by a peristaltic pump (Ismatec). Chronoamperometry (CA) at different cell voltages from 1.7 to 2.1 V was performed until a stable current was reached. Each potential measurement was recorded for 30 min. Electrochemical impedance spectroscopy (EIS) was measured under the catalytically relevant potential (1.7 V) in the frequency range from 100 kHz to 0.1 Hz, with 10 points per frequency decade and a perturbation wave of 10 mV.

Product Analysis and Data Processing

Ion chromatography (Metrohm 883 Basic) was used to analyze the concentration of the product in the electrolyte composition. A Metrosep C6 column was used for the quantification of NH_4^+ and a Metrosep Supp 5 column was used for the quantification of NO_2^- and NO_3^-.

The NH_3 and NO_2^- Faradaic efficiencies (*FE*'s) of the NO_3RR were calculated according to eqs 1 and 2.

$$FE_{NH_3} = \frac{nzF}{Q} = \frac{8 \times C_{NH_3} \times V \times F}{Q} \tag{1}$$

$$FE_{NO_2} = \frac{nzF}{Q} = \frac{2 \times C_{NO_2} \times V \times F}{Q} \tag{2}$$

Here, z = 8 and 2 represent the number of electron transfers required to form NH_3 and NO_2, n is the molar concentration of NH_3 and NO_2 in the catholyte stream, V is the volume of the catholyte stream, F is the Faraday constant, 96,485 C·mol^{-1}, and Q is the charge passing through the cell.

The single-pass conversion rate of NO_3^- was calculated based on eq 3:

$$X_{(NO_3^-)} = \frac{(C_{(NO_3^-)}^{(t=0)} - C_{(NO_3^-)}^{(t=30)})}{C_{(NO_3^-)}^{(t=0)}} \times 100 \tag{3}$$

where $C_{NO_3^-}^{t=0}$ represents the initial nitrate concentration and $C_{NO_3^-}^{t=30}$ represents the nitrate concentration after 30 min of reaction.

Electrochemical Active Surface Area Experiment

Copper underpotential deposition (Cu_{UPD}) was used to characterize the electrochemical active surface area (ECSA) of Ru/C and PVP-modified Ru/C catalysts.[47,48] Integration of the peak area corresponding to underpotential deposition (UPD) stripping allows the surface area to be calculated with the assumption of an adsorption ratio of a single Cu atom to each surface Ru metal atom and an electrosorption valency of +2.[49]

$$Cu_{upd} \rightarrow Cu^{2+} + 2e^- \quad 420\ \mu C \cdot cm^{-2} \tag{4}$$

All of the measurements were performed in a typical three-electrode cell. A graphite rod was used as the counter electrode, a reversible hydrogen electrode was used as the reference electrode, and a 5 mm glassy carbon electrode with the dropcast cathode catalyst was used as the working electrode. The catalyst ink was prepared in the same way as described previously, then 10 μL ink was dropcast on the glassy carbon electrode, and the electrode was dried. The obtained catalyst loading was 0.25 mg·cm^{-2}. All of the experiments were performed in 0.1 M H_2SO_4 and 2 mM Cu_2SO_4. Before all measurements, the electrolyte was purged with helium (He) for 20−30 min to remove the dissolved oxygen. First, cyclic voltammetry was performed for 20 cycles from 0.03 to 0.7 V at a scan rate of 10 mV·s^{-1} in 0.1 M H_2SO_4 to obtain the background. Then, the electrode was polarized at 0.29 V for 100 s in He-purged 2 mM Cu_2SO_4 and 0.1 M H_2SO_4 solution. After Cu deposition, a linear voltammetric scan was performed from 0.29 to 0.7 V at a scan rate of 10 mV·s^{-1} to oxidize all of the underpotential-deposited copper.

$$ECSA = \frac{Q_{Cu_{upd}}}{420\ \mu C \cdot cm^{-2} \times L_{Ru}} \tag{5}$$

where Q_{Cu} is the Cu_{UPD} stripping charge in μC·cm^{-2} and L_{Ru} is the Ru loading in the catalyst in g·m^{-2}.

Hydrogen Binding Energy

Ru has a strong interaction with hydrogen that leads to hydrogen underpotential deposition (H_{upd}), which means hydrogen adsorbs at positive potentials vs the reversible hydrogen electrode (RHE).[50,51] The hydrogen binding energy (HBE) is the descriptor of the hydrogen evolution reaction (HER).

Hydrogen binding energy (ΔG_H^0) is defined as

$$\frac{1}{2}H_2 + * \rightarrow H_{ad} \tag{6}$$

Hydrogen adsorption/desorption is given by

$$H^+ + e^- + * \rightarrow H_{ad} \tag{7}$$

Overall reaction:

$$H^+ + e^- \rightarrow \frac{1}{2}H_2 \tag{8}$$

The overall reaction could go through a Tafel−Volmer pathway, which is described as

$$\frac{1}{2}H_2 + M \rightleftarrows M - H_{ad} \quad \Delta G_1^0 = \Delta G_H^0 \tag{9}$$

$$M - H_{ad} \rightleftarrows H^+ + e^- + M \quad \Delta G_2^0 = -\Delta G_H^0 \tag{10}$$

For the second reaction, the H_{UPD} adsorption and desorption can be defined by $C-V$ profiles, ΔG_H^0 can be derived with reference to the H_{UPD} desorption peak (E_{peak}) in $C-V$ profiles, assuming a Langmuir adsorption isotherm, according to the following equation:

$$\Delta G_H^0 = -FE_{peak} \tag{11}$$

where F is the Faraday constant (96,485 C·mol^{-1}).[52,53]

Water Contact Angle Measurements

Water contact angle measurements were performed via the sessile drop method using an OCA 25 goniometer (DataPhysics Instruments GmbH, Filderstadt, Germany), and 2 μL of droplets were dispensed onto substrates using an automatic pipetting unit. Measurements were taken in ambient air in the temperature range of 20−24 °C (Figure S8).

RESULTS AND DISCUSSION

Promotional Effects of PVP on Ammonia Production over Ru/C Catalysts

We first synthesized Ru/C catalysts with different loadings (10, 20, and 40 wt %). The NO_3RR often has various byproducts. As per our observations, the nitrogen balance during the NO_3RR with the catalysts after varying potentials was considerably close (<5% loss, Figure S9). It is well known and also confirmed in this study that the hydrogen evolution reaction (HER) is the main competitive reaction.[20,26] Hydro-

https://doi.org/10.1021/acscatal.5c07637
ACS Catal. 2026, 16, 3430−3441

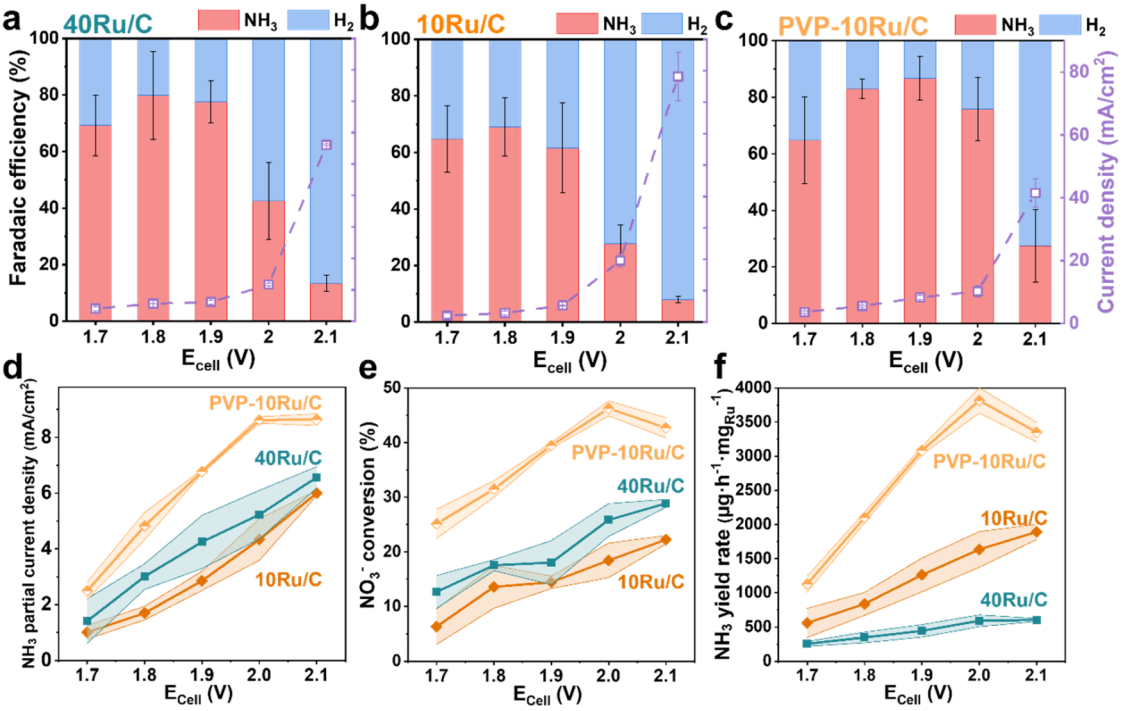

Figure 1. Electrochemical NO_3RR performance. Faradaic efficiency (*left*) and total current density (*right*) for electrochemical nitrate reduction on (a) 40Ru/C; (b) 10Ru/C, and (c) PVP-10Ru/C. (d) NH_3 partial current density, (e) NO_3^- single-pass conversion, and (f) NH_3 yield rate with regard to Ru metal loading.

gen and ammonia were the only two detectable products from the NO_3RR using the Ru/C electrocatalysts.

Figure 1a,b compares the electrocatalytic performance of 40Ru/C and 10Ru/C in the PEM electrolyzer, and the performance of 20Ru/C is shown in Figure S10a. A decrease in catalytic activity is observed upon reducing the Ru loading from 40 to 10 wt % on the carbon black support. The *FE* toward NH_3 first increases and then decreases within the tested cell voltage range, while the HER becomes dominant at higher voltages for all of the catalysts. The highest *FE*s toward NH_3 are 80% for 40Ru/C, 76% for 20Ru/C, and 69% for 10Ru/C at 1.9 V, respectively. Among all of the catalysts, 40Ru/C shows the highest *FE* toward NH_3. However, it should be noted that the total cell current densities are at a similar level, implying that a lower-Ru loading appears to reduce the ammonia synthesis efficiency, with a greater proportion of electrons being consumed by the competing HER, yielding H_2. As shown in Figure 1d and S10b, the NH_3 partial current density is higher with 40Ru/C than with 10Ru/C and 20Ru/C, indicating lower ammonia production with decreasing Ru metal loading. A similar trend can also be found in the NO_3^- single-pass conversion rate, where higher conversions are observed together with higher Ru metal loading (Figure 1e).

Polyvinylpyrrolidone (PVP) was introduced as a capping agent to engineer and control the size of Ru NPs, aiming to achieving higher activity and selectivity to NH_3 with lower-Ru loading on carbon black supports. To investigate the PVP effects systematically, PVP-modified Ru/C catalysts with the same loading were synthesized and tested under the same conditions as Ru/C catalysts for electrochemical nitrate reduction to ammonia. The Ru loading of all of the samples was measured by TGA (Table S1). Blank samples of PVP-modified carbon black (PVP-C) were also prepared using the same method. From the previous research in our group, we know that bare carbon black shows nearly no activity toward nitrate reduction to ammonia.[34] The control experiments with PVP-C (Figure S11a,b) also show that only a very small amount of ammonia formed with almost 100% nitrogen balances, indicating that PVP has no catalytic effect on the carbon support.

For the PVP-modified Ru/C catalysts, nitrogen balances were also calculated to verify the *FE* results (Figure S12), and nearly 100% of total nitrogen species were detected. Strikingly, PVP-10Ru/C shows the highest *FE* (86%) and reaches 46% NO_3^- single-pass conversion, which is the highest among all of the catalysts (Figure 1d). The electrocatalytic NO_3RR performance for PVP-20Ru/C and PVP-40Ru/C is depicted in Figure S13. The *FE* toward NH_3 decreases with increasing loading, showing the lowest NO_3^- conversion and NH_3 partial current density for PVP-40Ru/C, which indicate the limitation of the PVP medication method at high Ru loadings.

For better understanding the production rate regarding metal utilization, Figures 1f and S14 show the ammonia production rate with regard to Ru metal loading as a function of cell voltages. We observed that with PVP modification, Ru utilization is higher, leading to higher NH_3 production rates per mg Ru. Among all catalysts, PVP-10Ru/C remarkably shows the highest NH_3 yield of 3800 μg mg_{Ru}^{-1} h^{-1} at 2 V, compared to 590 μg mg_{Ru}^{-1} h^{-1} for 40Ru/C and 1636 μg mg_{Ru}^{-1} h^{-1} for 10Ru/C.

Exploring Structural and Electron Density Effects of PVP for Ru Nanoparticles

With PVP as a stabilizing agent, PVP-10Ru/C shows the highest performance for ammonia production on a Ru-based carbon-supported catalyst.

As shown in Figure 2a–c, the transmission electron microscopy (TEM) images of as-prepared PVP-10Ru/C, 10Ru/C, and 40Ru/C catalysts clearly indicate the decrease

https://doi.org/10.1021/acscatal.5c07637
ACS Catal. 2026, 16, 3430−3441

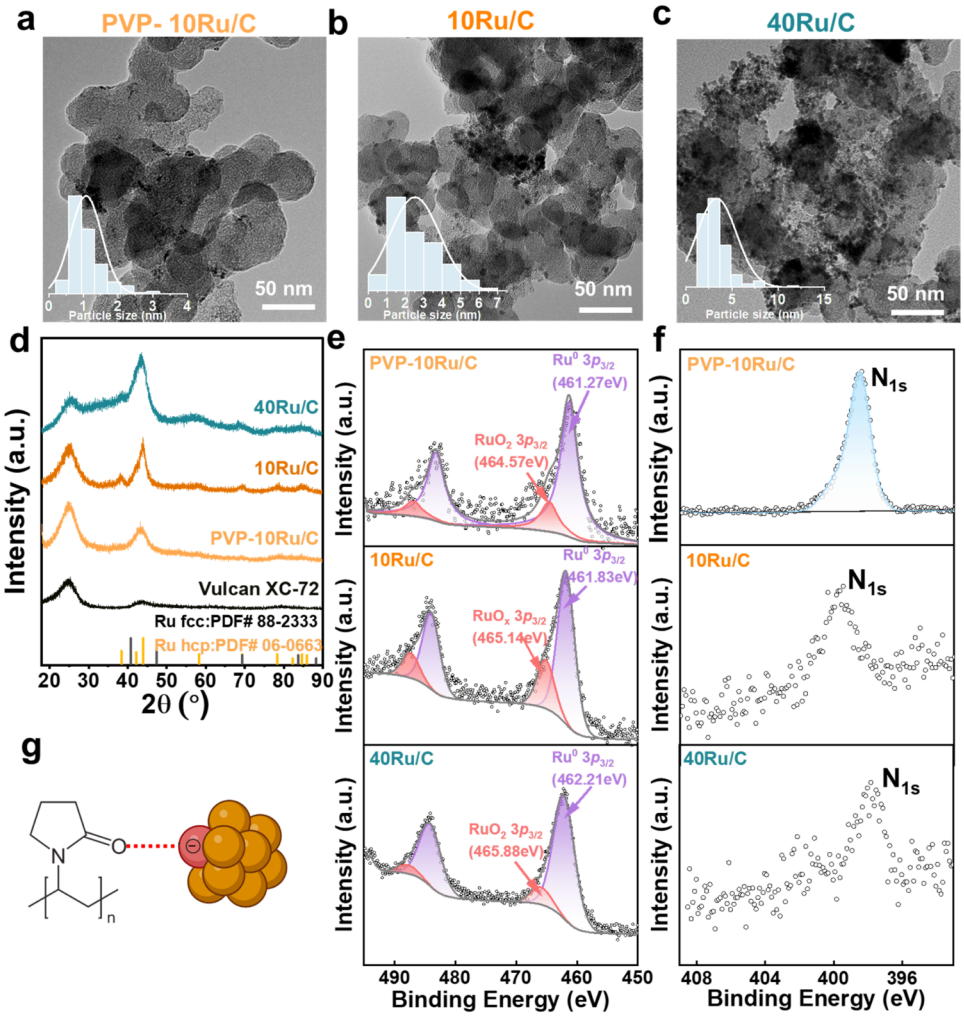

Figure 2. TEM images for (a) PVP-10Ru/C; (b) 10Ru/C; (c) 40Ru/C; (d) XRD patterns; (e) & (f) XPS data; (g) scheme of interaction between Ru and PVP.

in the size of Ru NPs. Size distributions were studied by analyzing 150 Ru NPs, resulting in average particle sizes of 3.2, 2.3, and 1.1 nm for 40Ru/C, 10Ru/C, and PVP-10Ru/C, respectively. For 40Ru/C, the Ru NP size ranges from 1 to 12 nm with evident aggregations. As the Ru loading is decreased to 20 wt %, the NP size range narrows to 0.5 to 10 nm, while some aggregations are still observed (Figure S15). Further reduction of the Ru loading to 10 wt % resulted in a particle size distribution of 0.5 to 8 nm with an approximate average size of 2.5 nm and with fewer aggregations. This shows that decreasing the Ru loading led to a reduction in the level of aggregate formation. In contrast, compared to bare Ru/C catalysts, the Ru NP size is clearly decreased for the PVP-modified Ru/C catalysts (Figures 2a and S16a). For PVP-20Ru/C and PVP-10Ru/C, the Ru NP particle size distributions are in the ranges of 0 to 4 and 0 to 3 nm, respectively, without obvious large aggregations, and the mean particle size distribution for PVP-10Ru/C is 1.1 nm. However, when the Ru loading is as high as 40 wt %, the presence of PVP cannot effectively prevent agglomeration (Figure S16b).

The X-ray diffraction (XRD) patterns (Figures 2d and S17) also suggest that the particle size of the PVP-modified Ru is smaller compared to the unmodified one. The broad diffraction peak around $2\theta = 25°$ is ascribed to the amorphous Vulcan XC72 carbon black support.[54] All Ru catalysts exhibited broad diffraction peaks around $2\theta = 44°$, which is attributed to metallic Ru (PDF#: 06-0663 and PDF#: 88-2333) and indicates a less-crystalline Ru structure rather than a well-faceted crystalline Ru.[55] Notably, the PVP-modified Ru/C catalysts display a distinct border peak in contrast to the Ru/C catalysts, indicating a smaller particle size of Ru NPs, which is in agreement with the TEM results.

The electronic structure and components of the as-prepared Ru-based catalysts were investigated by X-ray photoelectron spectroscopy. The XPS spectra of different loadings of 40Ru/C, 10Ru/C, and PVP-10Ru/C are presented in Figure 2e,f and for the rest of the studied catalysts are shown in Figure S18. The most intense C 1s peak was set at 284.6 eV as the reference for calibration.[56] The PVP-modified Ru/C catalysts show N 1s signals around 399−400 eV, which are attributed to the presence of N in PVP.[57] Conversely, no distinct N 1s signals are observed for as-prepared Ru/C catalysts, which confirm the incorporation of PVP in Ru/C electrocatalysts.

The electronic structure of Ru was investigated based on the binding energy (BE) of Ru 3p, due to a significant overlap between the Ru 3d and C 1s regions. XPS spectra of Ru 3p showed a doublet at the binding energies of 461 and 484 eV, corresponding to Ru 3p3/2 and Ru 3p1/2, respectively. For Ru 3p3/2, the peaks at binding energies of 462.21 and 465.88 eV represent the valence state of metallic Ru^0 and oxidized RuO_x,

https://doi.org/10.1021/acscatal.5c07637
ACS Catal. 2026, 16, 3430−3441

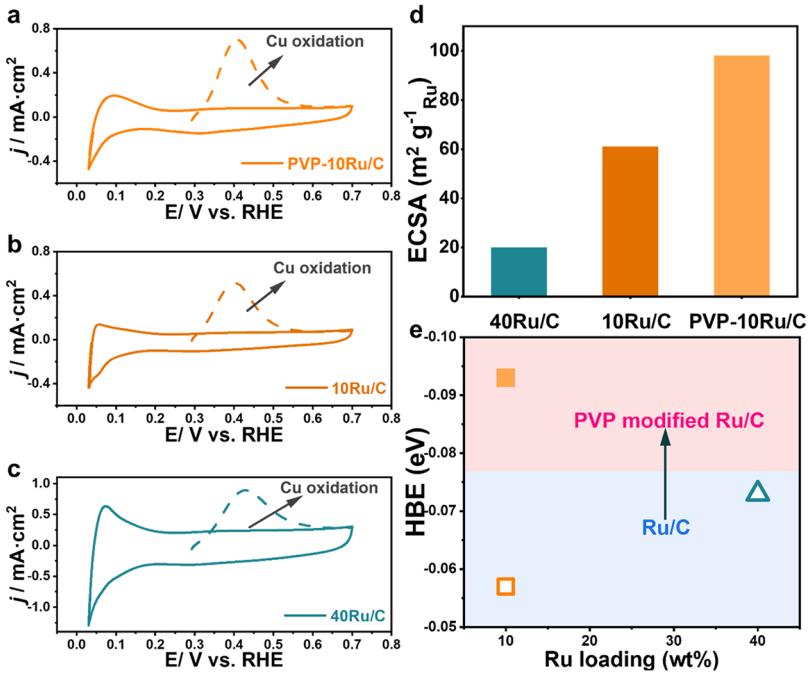

Figure 3. Cu_{UPD} voltammograms of (a) PVP-10Ru/C, (b) 10Ru/C, and (c) 40Ru/C. (d) ESCA and (e) HBE of PVP-10Ru/C, 10Ru/C, and 40Ru/C.

respectively. The presence of RuO_x suggests the formation of an oxide layer on the Ru surface when the catalyst is exposed to air. Table S2 shows the Ru 3p3/2 peak value of Ru/C and PVP-modified Ru/C. Negative shifts in binding energy were observed, which suggest the interaction between Ru NPs and PVP, where PVP serves as the electron donor and Ru is the electron acceptor (Figure 2g).[58] Interaction of PVP and Ru NPs leads to charge transfer from PVP to the Ru surface, resulting in a negative charge on the Ru surface, lowering the binding energy of Ru 3p orbitals. Similar observations of PVP decreasing metal binding energy were reported on Pt[58] and Au.[59] Additionally, the PVP-modified Ru catalysts exhibit higher electron density compared with unmodified Ru/C catalysts with smaller particle sizes. Overall, PVP-10Ru/C shows the lowest binding energy, indicating the highest electron density (Figure S19).

Electrochemical Characterization of Electrochemical Active Surface Area and Hydrogen Binding Energy

The electrochemical active surface area (ECSA) is a possible key descriptor in the NO_3RR. The copper underpotential deposition (Cu_{UPD}) stripping voltammetry method was used to investigate the ECSA of Ru catalysts with different particle sizes. Underpotential deposition (UPD) entails the adsorption of metal atoms onto an electrode surface, forming a monolayer or submonolayer at electrode potentials more positive than the potentials necessary for bulk deposition of the respective metal. Cu_{UPD} stripping voltammetry is an ideal method for measuring the ECSA of Ru due to the similarity of atomic radii for both metals, 0.128 and 0.134 nm for Cu and Ru, respectively.[47,60,61] As shown in Figure S20, the blank measurement represents the voltammogram obtained in a 0.1 M H_2SO_4 solution. To form the Cu UPD layers, the electrode was initially polarized at potentials 0.29, 0.285, 0.28, 0.275, and 0.27 V vs RHE for 100 s. Subsequently, the deposited Cu was oxidized between the deposition potential and 0.7 V vs RHE, using a sweep rate of 10 $mV \cdot s^{-1}$. Under polarization potentials of 0.29 V vs RHE, only one oxidation peak was observed around 0.4 V vs RHE, indicating the presence of a Cu monolayer. Another oxidation peak emerged while decreasing the polarization voltage, which is attributed to the oxidation of bulk copper. Therefore, the polarization voltage of 0.29 V vs RHE was employed in this study.

Figures 3a–d and S21 present that the PVP-modified and lower-Ru-loading electrocatalysts exhibited higher ECSA values compared to unmodified and higher-loading Ru/C catalysts. This suggests that the utilization efficiency of Ru metals was improved by downsizing the Ru NPs (Table S3). As expected, PVP-10Ru/C shows the largest ECSA value of 98 $m^2 \cdot g^{-1}$ among all of the synthesized catalysts. Compared with 40Ru/C and 10Ru/C catalysts, which show 25 $m^2 \cdot g^{-1}$ and 61 $m^2 \cdot g^{-1}$ ECSA values, PVP-10Ru/C exhibits a much higher value, almost 4 times higher than that of 40Ru/C.

To further elucidate the impact of PVP on Ru/C catalysts, the double-layer capacitance (C_{dl}) values were evaluated by cyclic voltammetry ($C-V$) over a non-faradic range, as depicted in Figure S22. The C_{dl} is the indicator of the accessibility of electrolyte ions to the electrode surface. Notably, the C_{dl} values for the PVP-modified Ru/C catalysts exceed those of the unmodified Ru/C catalysts. For instance, the C_{dl} value of PVP-10Ru/C is 30 $mF \cdot cm^{-2}$, compared to 23 $mF \cdot cm^{-2}$ of unmodified 10Ru/C. This trend is consistent over all of the Ru/C catalysts with 20 and 40 wt % loadings, further proving the enhancement in the exposure of Ru-active sites and the improved interaction between the electrolyte and the electrode with PVP modification.

Intriguingly, the electrochemical NO_3RR performance of the Ru/C catalysts (with or without PVP modification) was not consistent with the ECSA values. Among the Ru/C catalysts without PVP modification, 10Ru/C has a higher ECSA value and higher current density, but it shows lower *FE* toward NH_3 and lower NO_3^- conversion compared to 40Ru/C, which is unexpected. However, as expected, PVP-10Ru/C exhibits the

https://doi.org/10.1021/acscatal.5c07637
ACS Catal. 2026, 16, 3430−3441

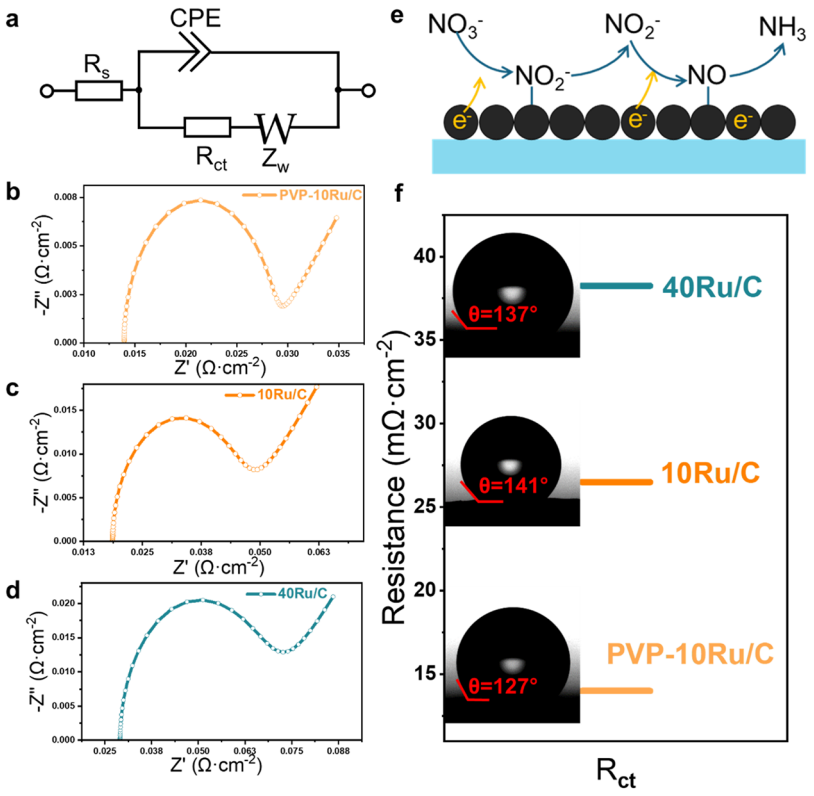

Figure 4. Electrochemical impedance spectroscopy (EIS). (a) Equivalent circuit used for EIS fitting; (b–d) fitted Nyquist plots of the EIS data of PVP-10Ru/C, 10Ru/C, and 40Ru/C; (e) illustration of charge transfer through the electrode surface; (f) water contact angle and charge-transfer resistance of PVP-10Ru/C, 10Ru/C, and 40Ru/C.

largest ECSA values together with the highest *FE* toward NH_3 and the highest NO_3^- conversion among all of the prepared Ru-based catalysts. Besides, the current density of PVP-10Ru/C was lower than those of Ru/C catalysts with same loading, which indicates the suppression of the HER in the reaction.

To further prove the above findings, it is of great importance to clarify the relationships among electrocatalytic NO_3RR performance, ECSA, and the HER. Thus, HBE was investigated as a descriptor for HER activity of the studied catalysts.[51,62] To this end, the HBE values were measured experimentally via *C*–*V* scans in blank solution (He-saturated 0.1 M H_2SO_4) from 0.03 to 0.7 V vs RHE at 10 mV·s^{-1} (Figure S23a–c). HBE was obtained from the H_{UPD} peak position (E_{peak}), which has a direct relationship with H_{UPD} using the equation: $\Delta G_H^0 = -FE_{Peak}$. According to the equation, the HBE values of the catalysts were calculated and summarized in Figures 3e, S23(d) and Table S3. It is widely accepted that the HER activity in the acid electrolyte is only determined by the HBE of the electrocatalyst surface.[60] Therefore, the higher HBE can be attributed to the decrease in HER activity of the Ru/C catalysts. For the Ru/C catalysts, the HBE decreases with decreasing Ru loading, indicating superior HER activity on 10Ru/C than 40Ru/C. This is consistent with the electrocatalytic performance of the NO_3RR that 10Ru/C shows higher current density with lower *FE* toward NH_3, and more electrons were utilized in the HER. As for the PVP-modified Ru/C catalysts, the HBE shows a higher value, which demonstrates inferior HER activity compared to Ru/C catalysts. PVP-10RuC with the highest HBE values displays the most suppression of the HER in comparison with all of the other catalysts. XPS spectra also show that the electronic structure of Ru modified by PVP shifts to a higher electron density. Previous research indicates that higher electron density can suppress the HER, which benefits from the nitrate reduction to ammonia formation.[63] Overall, the ECSA and HBE results confirm the importance of PVP in enhancing the active surface area and suppressing the hydrogen production.

Kinetic Investigations via Electrochemical Impedance Spectroscopy

Further, we investigated the effects of PVP on interfacial charge-transfer kinetics. Electrochemical impedance spectroscopy (EIS) was conducted under electrocatalytically relevant conditions at 1.7 V and used to study the charge transport and transfer phenomena on the electrode surface. The Randles equivalent circuit model (ECM) (Figure 4a) was constructed comprising Ohmic resistance (R_s), polarization charge-transfer resistance (R_{ct}) in the NO_3RR, and constant-phase elements (CPEs) which replace the electric double-layer capacitor to simulate the distribution of double-layer charging along the length of pores and the inhomogeneities on the porous electrode and a Warburg coefficient (W) considering the loss related with the diffusion process.[64,65] Among all of the elements in the ECM, R_{ct} represents the resistance encountered by ions crossing the electrode/electrolyte interface and inserting into the electrodes, which occurs at the solid–liquid contact area in the low-frequency region.[66,67] The NO_3RR takes place at the interface between the solid cathode electrode and the liquid electrolyte; hence, we focus on analyzing the R_{ct} to reveal the relation between charge-transfer kinetics at the electrode/electrolyte interface. The fitting results from EIS (Figures 4b–d and S24a–c) show that the

https://doi.org/10.1021/acscatal.5c07637
ACS Catal. 2026, 16, 3430–3441

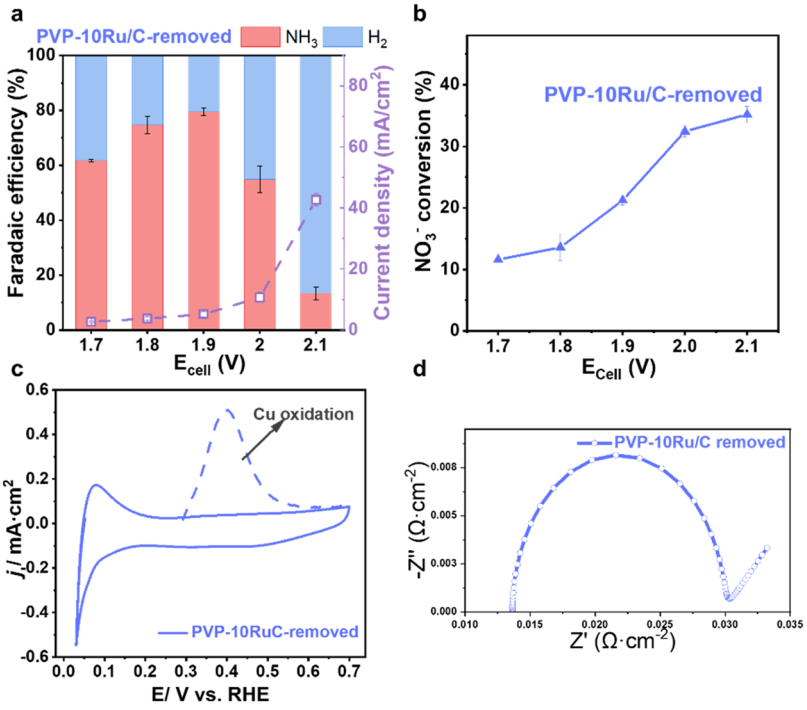

Figure 5. PVP-10Ru/C-removed catalyst. (a) Faradaic efficiency (*left*) and total current density (*right*) for electrochemical nitrate reduction; (b) NO_3^- conversion; (c) Cu_{UPD} voltammogram; (d) fitted Nyquist plots of the EIS data.

Ohmic resistances for different electrodes are at similar values. With regard to R_{ct} obtained from the ECM fitting (Figure 4e), as shown in Figure 4f, PVP-10Ru/C showed a significantly smaller value of 14 mΩ·cm^{-2}, compared to those of the 10Ru/C catalyst (26.5 mΩ·cm^{-2}) and 40Ru/C catalyst (38.3 mΩ·cm^{-2}). For the NO_3RR, smaller R_{ct} is more favorable for better charge-transfer kinetics. The EIS results show that the charge-transfer kinetics decreases substantially by decreasing the Ru metal loading with or without PVP modifications (Figure S24d and Table S4), which is in good agreement with the electronic structure modulation of Ru induced by the smaller particle size (Figure S19).

Moreover, PVP is a highly hydrophilic polymer,[68] which may improve the electrode wettability. The water contact angle results show that the PVP-modified catalysts have smaller contact angles (Figures 4f and S25), resulting in better wettability, which likely improves the ability of liquid electrolytes to spread out on the electrode surface and facilitates NO_3^- ion transportation through the interface. In summary, the EIS measurements further confirm the importance of PVP modification for enhanced charge-transfer kinetics and effective wetting area and ion transport.

Investigating the PVP Coverage Effects on Electrocatalytic Performance

To investigate whether PVP hinders electrocatalytic performance, a PVP removal experiment was conducted with the best-performing PVP-10Ru/C catalyst. To remove PVP efficiently, while keeping the same Ru particle size, the samples were heated to 300 °C in a N_2 atmosphere for 8 h. To further validate this, XRD, XPS spectroscopy, and TEM were used to characterize the PVP-10Ru/C-removed sample. As shown in Figure S26a, the PVP-10Ru/C-removed catalyst showed a significantly decreased N 1s peak intensity, which confirmed the effective removal of PVP but indicated that it cannot be removed completely. The XRD results (Figure S26b) still show a broad peak, indicating that the Ru NPs are still of small size. Moreover, TEM images show that the particle size distribution is similar to that of PVP-10Ru/C (Figure S26c). After removal of PVP in the PVP-10Ru/C catalyst, the binding energy of Ru 3p showed a similar level of 10Ru/C, which also indicated the successful removal of PVP without changing the Ru structure (Figure S26a).

The electrochemical NO_3RR experiments were performed under the same conditions as other catalysts, where we observe that the *FE* toward NH_3 (Figure 5a) and NO_3^- (Figure 5b) conversion is lower than that of PVP-10Ru/C. This indicates that more electrons are used to produce H_2. However, all of these values are slightly higher than that of 10Ru/C, showing that the remaining PVP likely plays a positive role in the electrocatalytic performance. Furthermore, the ECSA, HBE, and R_{ct} of the PVP-10Ru/C-removed catalyst (Table S5) is 74 m^2/g (Figure 5c), −0.079 eV (Figure 5c) and 16 mΩ/cm^2 (Figure 5d), respectively.

To decouple the particle size effect from the contribution of the capping agent and get a better understanding of PVP effects, 5 wt % Ru/C (named 5Ru/C) without PVP was synthesized as a control catalyst. By decreasing the metal loading, a similar mean particle size distribution (about 1.2 nm) was successfully achieved for 5Ru/C, as compared to the optimized PVP-10Ru/C (1.2 nm), which is confirmed by the particle size distribution from TEM measurement (Figure S27a). Figure S27b shows the electrochemical NO_3RR performance of 5Ru/C in a PEM electrolyzer, while Figure S27c confirms that the N balances are well closed, similar to other catalysts. The highest *FE* toward NH_3 is 55% at 1.8 V and decreased slightly to 51% at 1.9 V, which is inferior to the Ru-loading catalysts (10, 20, and 40 wt %) without PVP. Despite lower selectivity, the total cell current densities of 5Ru/C were comparable to, or slightly higher than, the other catalysts without PVP. This suggests that smaller Ru NPs result

https://doi.org/10.1021/acscatal.5c07637
ACS Catal. 2026, 16, 3430−3441

in a larger ECSA, which drives the high total current densities. However, a significant portion of this current contributes to the formation of H_2 instead of NH_3. This observation aligns with our main conclusion that decreasing the size of Ru NPs lowers the HBE, thereby promoting the HER and decreases the *FE* toward NH_3.

When normalizing the NH_3 yield rate by Ru metal loading (Figure S27d), PVP-10Ru/C shows the highest NH_3 production rate (3800 $\mu g\ mg_{Ru}^{-1}\ h^{-1}$ at 2 V), significantly outperforming 5Ru/C (2700 $\mu g\ mg_{Ru}^{-1}\ h^{-1}$). For the NO_3^- conversion rate (Figure S27e), PVP-10Ru/C shows the highest value, while 5Ru/C shows similar conversion to 10Ru/C, further confirming that the excess current in 5Ru/C is consumed by the HER.

Overall, the PVP removal experiments and the control experiments of NPs size-matched with 5Ru/C further confirm the significance of PVP for suppressing the HER and enhancing ammonia synthesis.

Tackling the Stability of PVP-Modified Ru/C Catalysts

PVP was introduced as a capping agent that can prevent Ru NP aggregation on a carbon support besides altering the electronic structure and wettability as described above. TEM images after the NO_3RR for all of the catalysts were taken to study the stability of Ru NPs on a carbon support. The results are summarized in Figures 6a–c and S28, exhibiting the particle size distribution of various Ru/C and PVP-modified Ru/C electrocatalysts before and after the NO_3RR.

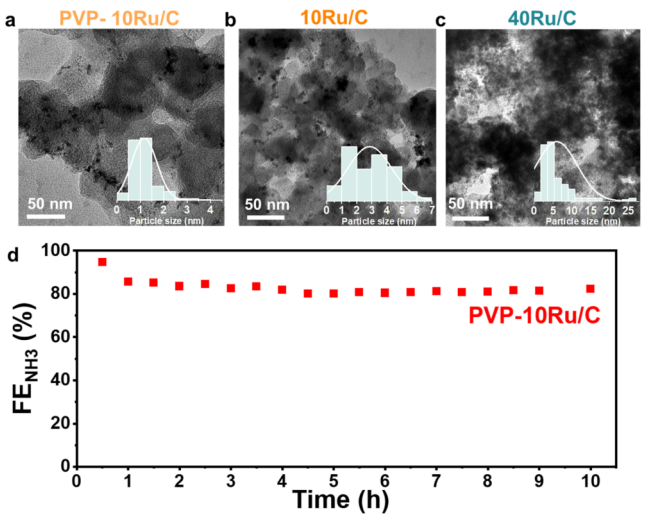

Figure 6. TEM images after the NO_3R reaction: (a) PVP-10Ru/C, (b) 10Ru/C, and (c) 40Ru/C. (d) *FE* toward NH_3 for PVP-10Ru/C as a function of time for 10 h.

Comparing the particle size distributions between Ru/C and PVP-modified Ru/C catalysts, the results showed a significant particle growth over Ru/C catalysts compared to PVP-modified catalysts. In the case of 40Ru/C, the particle size increased from 3.2 to 6.0 nm after the reaction; however, with PVP modification, the particle size only increased by 0.9 nm. For 10Ru/C, it can be observed that the Ru NPs agglomerated more prominently after the reaction compared with the PVP-modified one. The same observation also holds for 20Ru/C. All of the results indicated that PVP helps stabilize the particles during the electroreduction and prevent the agglomeration of Ru NPs, which result in better particle stability (Table S6).

For the practical application of an effective NO_3RR electrocatalyst, long-term durability is essential. We performed the stability test of PVP-10Ru/C at a constant voltage of 1.9 V for 10 h (Figure 6d). The *FE* toward NH_3 stabilized at around 82%, suggesting that PVP-10Ru/C has excellent stability for the NO_3RR to NH_3. Besides, the synthesis procedure is straightforward, containing only two steps: impregnation followed by sodium boron hydrate reduction, which offers significant potential for large-scale applications.

CONCLUSION

In conclusion, we have uncovered the promotion effect of PVP-modified Ru nanoparticles supported on carbon black for the NO_3RR to ammonia production and elucidated a 2-fold origin of this promotion effect. Electronically, PVP increases the electron density on the Ru surface, which suppresses the competing HER by increasing the hydrogen binding energy, thus further inhibiting the H–H formation. Physically, the PVP modification controls Ru nanoparticle size, which in turn amplifies the metal-utilization efficiency, increases the electrochemical active surface area, and improves charge transfer and hydrophilicity. As a result, PVP-10Ru/C exhibited outstanding performance, achieving a maximum NH_3 Faradaic efficiency of 86% and a single-pass NO_3^- conversion of 46% at 2 V. Notably, its NH_3 production rate is 3800 $\mu g\ mg_{Ru}^{-1}\ h^{-1}$ at 2 V, which is 6 times higher than that of the conventional 40 wt % Ru/C. Overall, the excellent electrocatalytic performance and a simple strategy of PVP modification can be a versatile method for developing superior electrocatalysts for demanding electrochemical reactions.

ASSOCIATED CONTENT

Supporting Information

The Supporting Information is available free of charge at https://pubs.acs.org/doi/10.1021/acscatal.5c07637.

Catalyst synthesis summary, PEM electrolyzer configuration and experimental setup, characterization results (TGA, TEM, XPS, XRD, and contact angle analysis), and electrochemical measurements (N balances, *C–V* for double-layer capacitance, control experiment, Cu_{UPD}, and EIS) (PDF)

AUTHOR INFORMATION

Corresponding Author

Atsushi Urakawa − *Department of Chemical Engineering, Delft University of Technology, Delft 2629 HZ, The Netherlands; e-Refinery Institute, Delft University of Technology, Delft 2628 CB, The Netherlands;* orcid.org/0000-0001-7778-4008; Email: A.Urakawa@tudelft.nl

Authors

Min Li − *Department of Chemical Engineering, Delft University of Technology, Delft 2629 HZ, The Netherlands; e-Refinery Institute, Delft University of Technology, Delft 2628 CB, The Netherlands*

Jinghan Zhao − *Department of Chemical Engineering, Delft University of Technology, Delft 2629 HZ, The Netherlands; e-Refinery Institute, Delft University of Technology, Delft 2628 CB, The Netherlands*

Vineesh Thazhe Veettil − *Department of Chemical Engineering, Delft University of Technology, Delft 2629 HZ,*

https://doi.org/10.1021/acscatal.5c07637
ACS Catal. 2026, 16, 3430−3441

The Netherlands; e-Refinery Institute, Delft University of Technology, Delft 2628 CB, The Netherlands; orcid.org/0000-0002-8559-2556

Shilong Fu − *Department of Process & Energy and e-Refinery Institute, Delft University of Technology, Delft 2628 CB, The Netherlands*

Ahmed Mohsen Ismail − *Department of Process & Energy and e-Refinery Institute, Delft University of Technology, Delft 2628 CB, The Netherlands;* Present Address: A.M.I. Department of Chemistry, Faculty of Science, Alexandria University, Alexandria, Egypt; orcid.org/0000-0002-6899-3577

Ruud Kortlever − *Department of Process & Energy and e-Refinery Institute, Delft University of Technology, Delft 2628 CB, The Netherlands;* orcid.org/0000-0001-9412-7480

Complete contact information is available at: https://pubs.acs.org/10.1021/acscatal.5c07637

Author Contributions

[‖]The manuscript was written through contributions of all authors. All authors have given approval to the final version of the manuscript. Authors M.L. and J.Z. contributed equally to this work.

Notes

The authors declare no competing financial interest.

■ ACKNOWLEDGMENTS

M.L. acknowledges the China Scholarship Council for this work.

■ REFERENCES

(1) Lehnert, N.; Dong, H. T.; Harland, J. B.; Hunt, A. P.; White, C. J. Reversing nitrogen fixation. *Nat. Rev. Chem.* **2018**, *2* (10), 278−289.

(2) Mahvi, A. H.; Nouri, J.; Babaei, A. A.; Nabizadeh, R. Agricultural activities impact on groundwater nitrate pollution. *Int. J. Environ. Sci. Technol.* **2005**, *2* (1), 41−47.

(3) Canfield, D. E.; Glazer, A. N.; Falkowski, P. G. The evolution and future of earth's nitrogen cycle. *Science* **2010**, *330* (6001), 192−196.

(4) Galloway, J. N.; Townsend, A. R.; Erisman, J. W.; Bekunda, M.; Cai, Z.; Freney, J. R.; Martinelli, L. A.; Seitzinger, S. P.; Sutton, M. A. Transformation of the nitrogen cycle: recent trends, questions, and potential solutions. *Science* **2008**, *320* (5878), 889−892.

(5) Wang, Z.; Richards, D.; Singh, N. Recent discoveries in the reaction mechanism of heterogeneous electrocatalytic nitrate reduction. *Catal. Sci. Technol.* **2021**, *11* (3), 705−725.

(6) Bijay, S.; Craswell, E. Fertilizers and nitrate pollution of surface and ground water: an increasingly pervasive global problem. *SN Appl. Sci.* **2021**, *3* (4), 518.

(7) Archna; Sharma, S. K.; Sobti, R. C. Nitrate removal from ground water: A review. *J. Chem.* **2012**, *9* (4), No. 154616.

(8) Xu, D.; Li, Y.; Yin, L.; Ji, Y.; Niu, J.; Yu, Y. Electrochemical removal of nitrate in industrial wastewater. *Front. Environ. Sci. Eng.* **2018**, *12* (1), 9.

(9) van Langevelde, P. H.; Katsounaros, I.; Koper, M. T. M. Electrocatalytic Nitrate Reduction for Sustainable Ammonia Production. *Joule* **2021**, *5* (2), 290−294.

(10) Wang, Y.; Xu, A.; Wang, Z.; Huang, L.; Li, J.; Li, F.; Wicks, J.; Luo, M.; Nam, D.-H.; Tan, C.-S.; et al. Enhanced Nitrate-to-Ammonia Activity on Copper−Nickel Alloys via Tuning of Intermediate Adsorption. *J. Am. Chem. Soc.* **2020**, *142* (12), 5702−5708.

(11) Pattabathula, V.; Richardson, J. Introduction to Ammonia Production. In *Chemical Engineering Progress*; American Institute of Chemical Engineers: New York, 2016; Vol. *112*, pp 69−75.

(12) Capdevila-Cortada, M. Electrifying the Haber−Bosch. *Nat. Catal.* **2019**, *2* (12), 1055.

(13) Service, R. F. New recipe produces ammonia from air, water, and sunlight. *Science* **2014**, *345* (6197), 610.

(14) Nørskov, J.; Chen, J.; Miranda, R.; Fitzsimmons, T.; Stack, R. Sustainable ammonia synthesis − exploring the scientific challenges associated with discovering alternative, sustainable processes for ammonia production. United States. 2016; Vol. *7* DOI: 10.2172/1283146.

(15) Wu, Z.-Y.; Karamad, M.; Yong, X.; Huang, Q.; Cullen, D. A.; Zhu, P.; Xia, C.; Xiao, Q.; Shakouri, M.; Chen, F.-Y.; et al. Electrochemical ammonia synthesis via nitrate reduction on Fe single atom catalyst. *Nat. Commun.* **2021**, *12* (1), No. 2870.

(16) Chen, G.-F.; Yuan, Y.; Jiang, H.; Ren, S.-Y.; Ding, L.-X.; Ma, L.; Wu, T.; Lu, J.; Wang, H. Electrochemical reduction of nitrate to ammonia via direct eight-electron transfer using a copper−molecular solid catalyst. *Nat. Energy* **2020**, *5* (8), 605−613.

(17) Fu, L.; Li, Y.; Yao, N.; Yang, F.; Cheng, G.; Luo, W. IrMo Nanocatalysts for Efficient Alkaline Hydrogen Electrocatalysis. *ACS Catal.* **2020**, *10* (13), 7322−7327.

(18) Wang, X.; Yao, H.; Zhang, C.; Li, C.; Tong, K.; Gu, M.; Cao, Z.; Huang, M.; Jiang, H. Double-Tuned RuCo Dual Metal Single Atoms and Nanoalloy with Synchronously Expedited Volmer/Tafel Kinetics for Effective and Ultrastable Ampere-Level Current Density Hydrogen Production. *Adv. Funct. Mater.* **2023**, *33* (40), No. 2301804.

(19) Wang, J.; Zang, W.; Liu, X.; Sun, J.; Xi, S.; Liu, W.; Kou, Z.; Shen, L.; Wang, J. Switch Volmer-Heyrovsky to Volmer-Tafel Pathway for Efficient Acidic Electrocatalytic Hydrogen Evolution by Correlating Pt Single Atoms with Clusters. *Small* **2024**, *20* (25), No. 2309427.

(20) Chen, F.-Y.; Wu, Z.-Y.; Gupta, S.; Rivera, D. J.; Lambeets, S. V.; Pecaut, S.; Kim, J. Y. T.; Zhu, P.; Finfrock, Y. Z.; Meira, D. M.; et al. Efficient conversion of low-concentration nitrate sources into ammonia on a Ru-dispersed Cu nanowire electrocatalyst. *Nat. Nanotechnol.* **2022**, *17* (7), 759−767.

(21) Wang, Y.; Li, H.; Zhou, W.; Zhang, X.; Zhang, B.; Yu, Y. Structurally Disordered RuO2 Nanosheets with Rich Oxygen Vacancies for Enhanced Nitrate Electroreduction to Ammonia. *Angew. Chem., Int. Ed.* **2022**, *61* (19), No. e202202604.

(22) Yang, R.; Li, H.; Long, J.; Jing, H.; Fu, X.; Xiao, J. Potential Dependence of Ammonia Selectivity of Electrochemical Nitrate Reduction on Copper Oxide. *ACS Sustainable Chem. Eng.* **2022**, *10* (43), 14343−14350.

(23) Cerrón-Calle, G. A.; Wines, A.; Garcia-Segura, S. Atomic hydrogen provision by cobalt sites in a bimetallic Ni/Co(OH)x and trimetallic Ni/Cu2O/Co(OH)x configurations for superior ammonia production. *Appl. Catal., B* **2023**, *328*, No. 122540.

(24) He, W.; Zhang, J.; Dieckhöfer, S.; Varhade, S.; Brix, A. C.; Lielpetere, A.; Seisel, S.; Junqueira, J. R. C.; Schuhmann, W. Splicing the active phases of copper/cobalt-based catalysts achieves high-rate tandem electroreduction of nitrate to ammonia. *Nat. Commun.* **2022**, *13* (1), No. 1129.

(25) Jeon, T. H.; Wu, Z.-Y.; Chen, F.-Y.; Choi, W.; Alvarez, P. J. J.; Wang, H. Cobalt−Copper Nanoparticles on Three-Dimensional Substrate for Efficient Ammonia Synthesis via Electrocatalytic Nitrate Reduction. *J. Phys. Chem. C* **2022**, *126* (16), 6982−6989.

(26) Li, J.; Zhan, G.; Yang, J.; Quan, F.; Mao, C.; Liu, Y.; Wang, B.; Lei, F.; Li, L.; Chan, A. W. M.; et al. Efficient Ammonia Electrosynthesis from Nitrate on Strained Ruthenium Nanoclusters. *J. Am. Chem. Soc.* **2020**, *142* (15), 7036−7046.

(27) Tan, H.; Tian, Y.; Peng, W.; Liu, X.; Wang, L.; Peng, Y.; Wang, C.; Liang, J.; Yan, X. Advances in Electrocatalytic Nitrate Reduction: Insights into Mechanisms and Reaction Optimization. *Adv. Sustainable Syst.* **2025**, *9* (11), No. 2400934.

(28) Chen, W.; Wang, L.; Wang, Y.; Sun, Z.; Liu, M.; Shang, H.; Wang, R.; Yang, C.; Wang, D.; Chen, W.; Zang, S.-Q. Atomic-Level Modulation of N-Bridge-Induced Built-In Electric Fields for

Enhanced Hydrogen Spillover in Ammonia Electrosynthesis. *ACS Catal.* **2025**, *15* (19), 16493−16505.
(29) Ye, D.; Tsang, S. C. E. Prospects and challenges of green ammonia synthesis. *Nat. Synth.* **2023**, *2* (7), 612−623.
(30) John, J.; MacFarlane, D. R.; Simonov, A. N. The why and how of NOx electroreduction to ammonia. *Nat. Catal.* **2023**, *6* (12), 1125−1130.
(31) Wu, T.; Han, M.-Y.; Xu, Z. J. Size Effects of Electrocatalysts: More Than a Variation of Surface Area. *ACS Nano* **2022**, *16* (6), 8531−8539.
(32) Speck, F. D.; Paul, M. T. Y.; Ruiz-Zepeda, F.; Gatalo, M.; Kim, H.; Kwon, H. C.; Mayrhofer, K. J. J.; Choi, M.; Choi, C. H.; Hodnik, N.; Cherevko, S. Atomistic Insights into the Stability of Pt Single-Atom Electrocatalysts. *J. Am. Chem. Soc.* **2020**, *142* (36), 15496−15504.
(33) Roy, C.; Sebok, B.; Scott, S. B.; Fiordaliso, E. M.; Sørensen, J. E.; Bodin, A.; Trimarco, D. B.; Damsgaard, C. D.; Vesborg, P. C. K.; Hansen, O.; et al. Impact of nanoparticle size and lattice oxygen on water oxidation on NiFeOxHy. *Nat. Catal.* **2018**, *1* (11), 820−829.
(34) Holby, E. F.; Sheng, W.; Shao-Horn, Y.; Morgan, D. Pt nanoparticle stability in PEM fuel cells: influence of particle size distribution and crossover hydrogen. *Energy Environ. Sci.* **2009**, *2* (8), 865−871.
(35) Li, S.; Han, D.; Jiang, G.; Han, Z.; Lu, H.; Gao, J.; Wang, X.; Wang, Y.; Geng, C.; Weng, Z.; Yang, Q.-H. Proton Exchange Membrane Electrode Assembly for Ammonia Electrosynthesis from Nitrate. *ACS Appl. Energy Mater.* **2023**, *6* (9), 5067−5073.
(36) Bunea, S.; Clemens, K.; Urakawa, A. Electrified Conversion of Contaminated Water to Value: Selective Conversion of Aqueous Nitrate to Ammonia in a Polymer Electrolyte Membrane Cell. *ChemSusChem* **2022**, *15* (2), No. e202102180.
(37) Ampurdanés, J.; Bunea, S.; Urakawa, A. PEM Electrolysis-Assisted Catalysis Combined with Photocatalytic Oxidation towards Complete Abatement of Nitrogen-Containing Contaminants in Water. *ChemSusChem* **2021**, *14* (6), 1534−1544.
(38) Yuan, T.; Li, M.; Subramanian, S.; Kok, J.; Li, M.; Urakawa, A.; Voznyy, O.; Burdyny, T. Sequential electrocatalytic reactions along a membrane electrode assembly drive efficient nitrate-to-ammonia conversion. *Cell Rep. Phys. Sci.* **2024**, *5* (6), No. 101977.
(39) Huang, P.-W.; Song, H.; Yoo, J.; Chipoco Haro, D. A.; Lee, H. M.; Medford, A. J.; Hatzell, M. C. Impact of Local Microenvironments on the Selectivity of Electrocatalytic Nitrate Reduction in a BPM-MEA System. *Adv. Energy Mater.* **2024**, *14* (28), No. 2304202.
(40) Kyrychenko, A.; Korsun, O. M.; Gubin, I. I.; Kovalenko, S. M.; Kalugin, O. N. Atomistic simulations of coating of silver nanoparticles with poly(vinylpyrrolidone) oligomers: effect of oligomer chain length. *J. Phys. Chem. C* **2015**, *119* (14), 7888−7899.
(41) Ilinitch, O. M.; Cuperus, F. P.; Nosova, L. V.; Gribov, E. N. Catalytic membrane in reduction of aqueous nitrates: operational principles and catalytic performance. *Catal. Today* **2000**, *56* (1), 137−145.
(42) Wu, S.; Sun, W.; Chen, J.; Zhao, J.; Cao, Q.; Fang, W.; Zhao, Q. Efficient imine synthesis from oxidative coupling of alcohols and amines under air atmosphere catalysed by Zn-doped Al2O3 supported Au nanoparticles. *J. Catal.* **2019**, *377*, 110−121.
(43) Lopez-Sanchez, J. A.; Dimitratos, N.; Hammond, C.; Brett, G. L.; Kesavan, L.; White, S.; Miedziak, P.; Tiruvalam, R.; Jenkins, R. L.; Carley, A. F.; et al. Facile removal of stabilizer-ligands from supported gold nanoparticles. *Nat. Chem.* **2011**, *3* (7), 551−556.
(44) Rioux, R. M.; Song, H.; Grass, M.; Habas, S.; Niesz, K.; Hoefelmeyer, J. D.; Yang, P.; Somorjai, G. A. Monodisperse platinum nanoparticles of well-defined shape: synthesis, characterization, catalytic properties and future prospects. *Top. Catal.* **2006**, *39* (3), 167−174.
(45) Armenise, S.; Cazaña, F.; Monzón, A.; García-Bordejé, E. In situ generation of CO_x-free H_2 by catalytic ammonia decomposition over Ru-Al-monoliths. *Fuel* **2018**, *233*, 851−859.
(46) Kim, T. W.; Oh, J.; Suh, Y.-W. Hydrogenation of 2-benzylpyridine over alumina-supported Ru catalysts: Use of $Ru_3(CO)_{12}$ as a Ru precursor. *Appl. Catal., A* **2017**, *547*, 183−190.
(47) Green, C. L.; Kucernak, A. Determination of the platinum and ruthenium surface areas in platinum−ruthenium electrocatalysts by underpotential deposition of copper. 2. effect of surface composition on activity. *J. Phys. Chem. B* **2002**, *106* (44), 11446−11456.
(48) Green, C. L.; Kucernak, A. Determination of the platinum and ruthenium surface areas in platinum−ruthenium alloy electrocatalysts by underpotential deposition of copper. I. unsupported catalysts. *J. Phys. Chem. B* **2002**, *106* (5), 1036−1047.
(49) Machado, S. A. S.; Tanaka, A. A.; Gonzalez, E. R. Underpotential deposition of copper and its influence in the oxygen reduction on platinum. *Electrochim. Acta* **1991**, *36* (8), 1325−1331.
(50) Karlberg, G. S.; Jaramillo, T. F.; Skúlason, E.; Rossmeisl, J.; Bligaard, T.; Nørskov, J. K. Cyclic voltammograms for H on Pt(111) and Pt(100) from first principles. *Phys. Rev. Lett.* **2007**, *99* (12), No. 126101.
(51) Hu, Q.; Gao, K.; Wang, X.; Zheng, H.; Cao, J.; Mi, L.; Huo, Q.; Yang, H.; Liu, J.; He, C. Subnanometric Ru clusters with upshifted D band center improve performance for alkaline hydrogen evolution reaction. *Nat. Commun.* **2022**, *13* (1), No. 3958.
(52) Wang, Q.; Xu, C.-Q.; Liu, W.; Hung, S.-F.; Bin Yang, H.; Gao, J.; Cai, W.; Chen, H. M.; Li, J.; Liu, B. Coordination engineering of iridium nanocluster bifunctional electrocatalyst for highly efficient and pH-universal overall water splitting. *Nat. Commun.* **2020**, *11* (1), No. 4246.
(53) Zheng, J.; Nash, J.; Xu, B.; Yan, Y. Perspective-towards establishing apparent hydrogen binding energy as the descriptor for hydrogen oxidation/evolution reactions. *J. Electrochem. Soc.* **2018**, *165* (2), No. H27.
(54) Ungár, T.; Gubicza, J.; Ribárik, G.; Pantea, C.; Zerda, T. W. Microstructure of carbon blacks determined by X-ray diffraction profile analysis. *Carbon* **2002**, *40* (6), 929−937.
(55) Lee, W.-J.; Bera, S.; Woo, H.-J.; An, J.-W.; Bae, J.-S.; Oh, I.-K.; Kwon, S.-H. Controllable size and crystallinity of Ru nanoparticles on a carbon support synthesized by fluidized bed reactor-atomic layer deposition for enhanced hydrogen oxidation activity. *J. Mater. Chem. A* **2021**, *9* (32), 17223−17230.
(56) Awasthi, M. K.; Rai, R. K.; Behrens, S.; Singh, S. K. Low-temperature hydrogen production from methanol over a ruthenium catalyst in water. *Catal. Sci. Technol.* **2021**, *11* (1), 136−142.
(57) Hantsche, H. *High Resolution XPS of Organic Polymers, the Scienta ESCA300 Database*; John Wiley & Sons, Ltd, 1993 DOI: 10.1002/adma.19930051035.
(58) Ye, J.-Y.; Attard, G. A.; Brew, A.; Zhou, Z.-Y.; Sun, S.-G.; Morgan, D. J.; Willock, D. J. Explicit Detection of the Mechanism of Platinum Nanoparticle Shape Control by Polyvinylpyrrolidone. *J. Phys. Chem. C* **2016**, *120* (14), 7532−7542.
(59) Haesuwannakij, S.; Kimura, T.; Furutani, Y.; Okumura, K.; Kokubo, K.; Sakata, T.; Yasuda, H.; Yakiyama, Y.; Sakurai, H. The Impact of the Polymer Chain Length on the Catalytic Activity of Poly(N-vinyl-2-pyrrolidone)-supported Gold Nanoclusters. *Sci. Rep.* **2017**, *7* (1), No. 9579.
(60) Moffat, T. P.; Walker, M.; Chen, P. J.; Bonevich, J. E.; Egelhoff, W. F.; Richter, L.; Witt, C.; Aaltonen, T.; Ritala, M.; Leskelä, M.; Josell, D. Electrodeposition of Cu on Ru Barrier Layers for Damascene Processing. *J. Electrochem. Soc.* **2006**, *153* (1), No. C37.
(61) Bogolowski, N.; Huxter, S.; Abd-El-Latif, A.-E.-A. A.; Attard, G. A.; Baltruschat, H. Copper underpotential deposition on Ru quasi-single-crystal films. *J. Electroanal. Chem.* **2010**, *646* (1), 68−74.
(62) Shi, Y.; Ma, Z.-R.; Xiao, Y.-Y.; Yin, Y.-C.; Huang, W.-M.; Huang, Z.-C.; Zheng, Y.-Z.; Mu, F.-Y.; Huang, R.; Shi, G.-Y.; et al. Electronic metal−support interaction modulates single-atom platinum catalysis for hydrogen evolution reaction. *Nat. Commun.* **2021**, *12* (1), No. 3021.
(63) Wang, Y.; Zhou, W.; Jia, R.; Yu, Y.; Zhang, B. Unveiling the Activity Origin of a Copper-based Electrocatalyst for Selective Nitrate

Reduction to Ammonia. *Angew. Chem., Int. Ed.* **2020**, *59* (13), 5350−5354.
(64) Zhao, X.; Zhou, Y.; Wang, L.; Pan, B.; Wang, R.; Wang, L. Classification, summarization and perspective on modeling techniques for polymer electrolyte membrane fuel cell. *Int. J. Hydrogen Energy* **2023**, *48* (57), 21864−21885.
(65) Yuan, X.-Z.; Song, C.; wang, H.; Zhang, J.*Electrochemical Impedance Spectroscopy in PEM Fuel Cells* 2010 DOI: 10.1007/978-1-84882-846-9.
(66) Lou, F.; Chen, D. Aligned carbon nanostructures based 3D electrodes for energy storage. *J. Energy Chem.* **2015**, *24* (5), 559−586.
(67) Zhang, D.; Nagayama, G. Effective Wetting Area Based on Electrochemical Impedance Analysis: Hydrophilic Structured Surface. *Langmuir* **2019**, *35* (50), 16508−16513.
(68) Tiron, L. G.; Vlad, M.; Baltă, Ş. Research on Hydrophilic Nature of Polyvinylpyrrolidone on Polysulfone Membrane Filtration. *IOP Conf. Ser.: Mater. Sci. Eng.* **2018**, *374* (1), No. 012059.

https://doi.org/10.1021/acscatal.5c07637
ACS Catal. 2026, 16, 3430−3441